AIAA JOURNAL
Vol. 33, No. 4, April 1995

Compressible Inviscid Vortex Flow of a Sharp Edge Delta Wing

J. M. A. Longo*
DLR, German Aerospace Research Establishment, D-38108 Braunschweig, Germany

An analysis is presented on the compressible inviscid vortex flow over three delta wings with sharp leading edges with leading edge sweep angles φ = 60, 70, and 76 deg using numerical solutions of the Euler equations. Presentations of results are given for Mach numbers ranging from M_∞ = 0.1 to 0.8 and for angles of attack up to the onset of vortex breakdown. The paper focuses the attention on the effects of the vortex flow on the flowfield of a delta wing. The occurrence of shock waves of two types, crossflow and terminating (or rear) shocks in the vortical flowfields, are investigated; the possibility of shock-induced vortex breakdown and the effects of compressibility on the rapid performance degradation of delta wings after vortex bursting are studied in detail. It is shown that the onset of the vortex bursting at the wing trailing edge is only weakly influenced by the freestream Mach number. The upstream progression of the vortex bursting, however, is faster for supersonic vortex cores. For transonic flows, terminating shocks are observed downstream of vortex bursting. Crossflow shocks, however, may already develop for low-subsonic freestream Mach numbers. Also, it is found that the core flow is already compressible for freestream Mach numbers $M_\infty \approx 0.1$ and that significant amounts of entropy and circulation are generated within the core.

Nomenclature

C_D	= drag coefficient
C_L	= lift coefficient
C_M	= pitching moment coefficient
C_p	= static pressure coefficient
C_{pt}	= total pressure loss coefficient
M	= Mach number
p	= static pressure
S	= entropy, also path along a surface streamline according to Fig. 10.
$\bar{U}$	= velocity vector on a body-fixed coordinate system
u, v, w	= velocity components on a vortex axis-oriented coordinate system
u_1, u_2, u_3	= velocity components on a body-fixed coordinate system
$\bar{V}$	= velocity vector on a vortex axis-oriented coordinate system
x, y, z	= vortex axis-oriented coordinate system
x_1, x_2, x_3	= body-fixed coordinate system
α	= angle of attack
Γ	= circulation, $(2\pi r)^{-1} \int \bar{U} \cdot \overline{dl}$
$\gamma_x, \gamma_y, \gamma_z$	= vorticity components on a vortex axis-oriented coordinate system
κ	= ratio of the specific heats
ξ, η, ζ	= nondimensional body-fixed coordinate system
ρ	= density
φ	= wing leading-edge swept angle
$\bar{\Omega}$	= vorticity vector on a vortex axis-oriented coordinate system

Subscripts

n	= normal to the wing leading edge
∞	= freestream conditions

Introduction

THE vortical flowfield generated around sharp-edged delta wings at high angle of attack has been the subject of numerous research activities in the last 50 years. Most of the existing investigations, however, were carried out at subsonic or supersonic conditions, as is shown from the excellent comprehensive reviews published by Hoeijmakers[1] and Newsome and Kandil.[2] Experimental investigations at transonic freestream Mach numbers[3,4] have shown a complicated flowfield with crossflow shocks, terminating or rear shocks and leading-edge shocks partially embedded in the flowfield which is generated by the leading-edge vortices. The influence of the shocks on the breakdown of the vortices and on the degradation of the aerodynamics performances of the delta wing after vortex bursting is still unknown. Similarly, other questions related to the physics of the compressible flow within the vortex core remain until now unanswered. Although Navier–Stokes solutions were shown to be qualitatively and also quantitatively more accurate than Euler results[5,6] the improvements of the solution are restricted to secondary effects. Today numerical methods based on the solution of the Euler equations have reached sufficient maturity to be used to describe essential flow features such as the production of vortex lift, the interaction between shock and vortices, and the prediction of vortex breakdown. The interested reader is referred to many papers published during recent years.[6–16] To contribute to a better understanding of the compressible vortex flow fields of sharp-edged delta wings, a systematic study using the DLR CEVCATS Euler code is reported in the present work. Three delta wings with sharp leading edges, with sweep angles of $\varphi = 60$, 70, and 76 deg are studied for $0.1 \leq M_\infty \leq 0.8$, and for angles of attack up to vortex breakdown.

Numerical Approach

Computer Code

The simulations of the flowfield are done by means of solutions of the Euler equations, representing conservation of mass, momentum, and energy. The numerical solutions are computed with the DLR CEVCATS Euler code. The description of the basic solution method for the numerical algorithm is given in Refs. 17–19. The computational algorithm employs a finite volume spatial discretization, in which the discrete values of the flow quantities are located at the vertices of the mesh cell. Artificial dissipative terms (also known as artificial viscosity) based on the work of Jameson et al.[20] are added to the governing discrete equations. The magnitudes of these terms depend on the pressure gradients in the flow and damping coefficients k^2 and k^4 specified by the user. Typical values for these user-specified coefficients are $k^2 = 1/2$ and $k^4 = 1/32$ or 1/64. Small values imply less numerical dissipation in the solutions but also less stability margin for the numerical scheme. Earlier studies[10] on vortical flow simulation with Euler codes showed that the use of a high amount of numerical dissipation produces solutions with a large error in the values of the density. Hence, for the present study

Received Nov. 23, 1993; presented as Paper 94-0071 at the AIAA 32nd Aerospace Sciences Meeting, Reno, NV, Jan. 10–13, 1994; revision received Aug. 3, 1994; accepted for publication Aug. 31, 1994.

*Reasearch Scientist, Institute of Design Aerodynamic. Member AIAA.

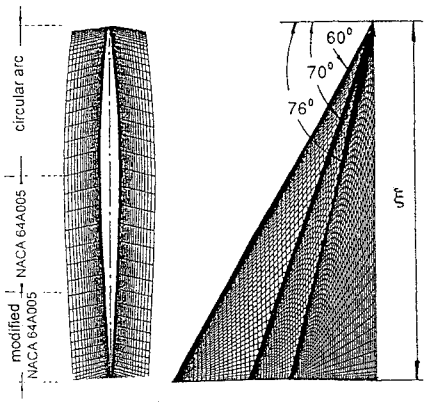

Fig. 1a Configurations.

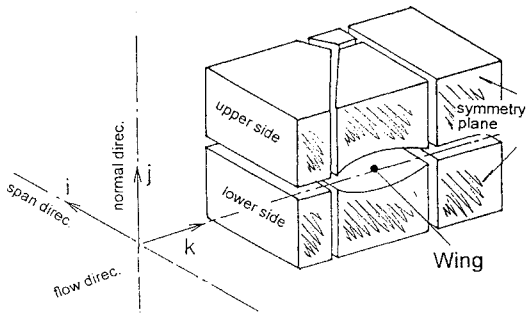

Fig. 1b Grid structure.

minimum values of the dissipation coefficients k^2 and k^4 allowed by the convergence of the solution on the given grids are used, i.e., $k^2 = 1/4$ and $k^4 = 1/128$–$1/256$. The system of ordinary differential equations which is obtained by the discretization in space is advanced in time with a five-stage Runge–Kutta scheme. Three methods are used to accelerate convergence to steady state, local time stepping, implicit smoothing of the residuals, and a multigrid method. The code allows multiblock decomposition of the computational domain and it is, therefore, grid topology independent. The required computer time for each angle of attack and or Mach number is less than 15 min. for steady-state solutions and about 30 min. in presence of vortex breakdown on a CRAY-YMP computer. This time includes the time required to read and write data files as well as the time required to perform the calculations.

Configurations and Grid

In the present study three delta wings with sharp leading edges and leading-edge sweep angles of $\varphi = 60$, 70, and 76 deg and symmetric wing profiles (Fig. 1a) are numerically tested. The physical domain is discretized by means of an eight-block H–H topology grid consisting of 460,000 points (Fig. 1b). This topology structure offers high flexibility to geometrical changes of the configuration without altering the whole domain. On each block the mesh is generated in three main steps[16]: first a three-dimensional body-fitted grid is generated via transfinite interpolation, then a two-dimensional elliptic solver is applied on each block face, finally a three-dimensional elliptic solver is used to smooth the grid inside each block enforcing orthogonality of the grid lines at block boundaries, which prevents solutions from spurious vortex bursting at block boundaries due to grid skewness. About 4600 points are used to discretized the wing surfaces. The outer boundaries of the computational domain extend approximately 6 wing root chords in all directions. The clustering of grid lines in direction normal to the surface of the configuration has a minimum spacing for the first mesh layer of $\leq 10^{-3}$ chord lengths.

Computation of Vortex Bursting

The governing equations and computational algorithms used for this investigation were formulated to achieve steady-state solutions. The criterion used to determine when the solution converged to its steady state is the residual convergence of the continuity equation, namely, the L_2 norm. Converged solutions are assumed once the L_2 norm drops at least through three orders of magnitude. A different time interval is used in each cell to accelerate the convergence to steady state and, hence, the discrete equations are not solved in a time-accurate fashion. Once the vortex bursts, the flowfield induced by the vortex becomes unsteady. At the location of the vortex bursting and downstream this point along the vortex axis, the computed flow variables (i.e., density, velocity, and internal energy) do not converge to a steady state but they exhibit an oscillatory motion of periodic character. About one-third of the time steppings required to obtain a steady-state solution are necessary to complete one period of the oscillatory motion. Hence, for flow conditions corresponding to vortex bursting, the solutions are not diverging. They have converged to results which are globally stationary but locally unsteady and, hence, converged solutions are assumed once the computed flow variables reach in terms of their mean values the steady state. Since once the vortex bursts the velocity profile of the axial component of the core flow changes its character from jet type to wake type, vortex breakdown is defined in the present work as the place where the second derivative of the axial component of the core flow with respect to the core radius is zero (i.e., $\partial^2 u/\partial r^2 = 0$). This procedure for the computation of vortical flows up to vortex breakdown has been successfully applied in previous numerical studies.[6,12,16] Figure 2 shows computed forces, and pitching moment and the progression of the bursting with incidence for a delta wing $\varphi = 60$ deg correlated with experimental data.[21–23] It turn out that the present technique is able to describe the basic effects of the vortical flow on the aerodynamics characteristics of sharp-edged delta wings. Extensive numerical–experimental correlation studies were published in Ref. 16.

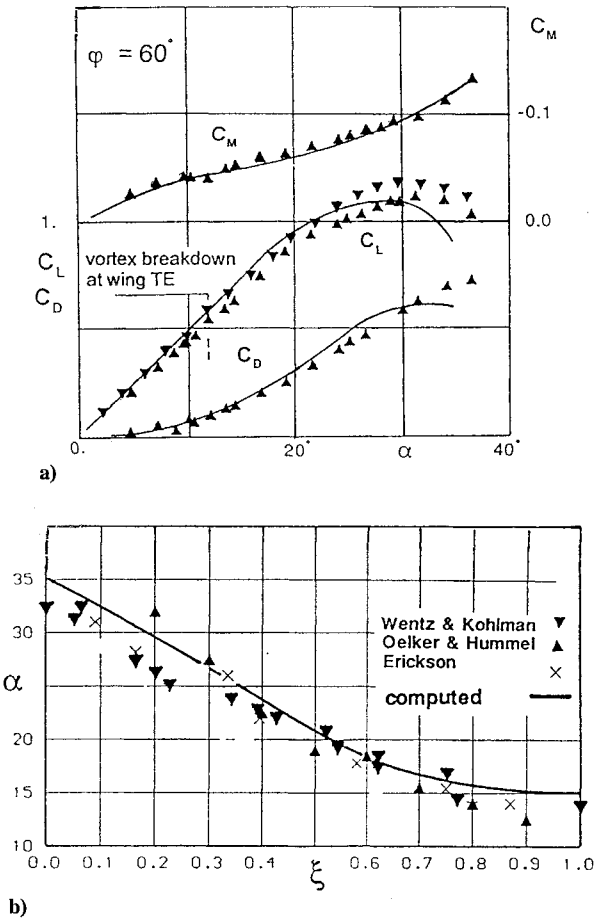

Fig. 2 Numerical–experimental correlation for vortical flow aerodynamics up to vortex breakdown for a wing $\varphi = 60$ deg, $M_\infty \approx 0.1$.

Results and Discussion

Forces and Pitching Moments

Aerodynamics forces and pitching moments for the three delta wings for two freestream Mach numbers, 0.4 and 0.8, are shown

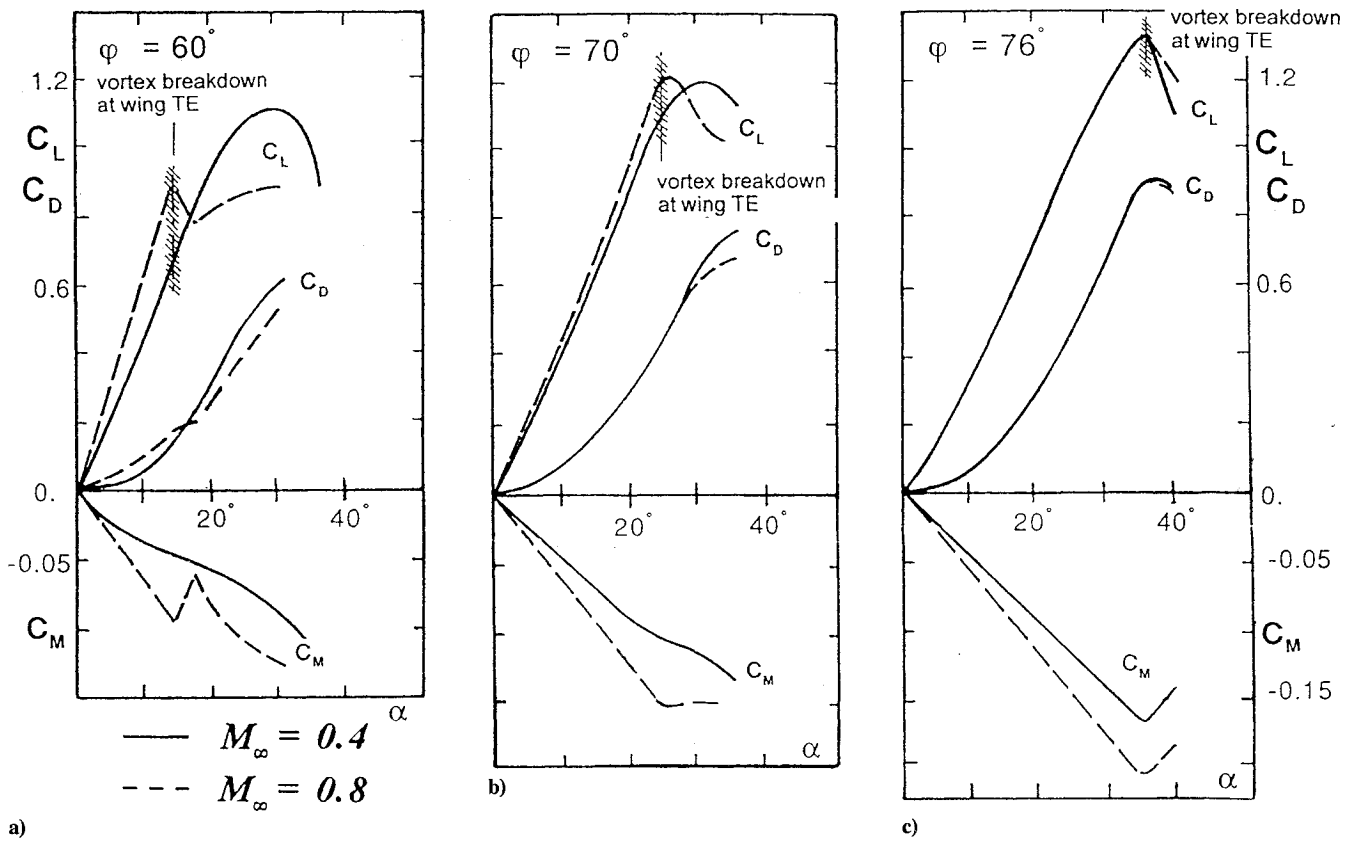

Fig. 3 Forces and moments.

in Fig. 3. Values of forces and moments were computed using an increment on angle of attack of $\Delta\alpha = 5$ deg. Maximum values and or discontinuities on each curve were explored using a $\Delta\alpha \approx 1$ deg. It is shown that the effect of the Mach number on the total forces and pitching moment is larger for delta wings with small sweep. Also, as the wing leading-edge sweep angle increases, the slope of the lift curves decreases due to the reduction of the wing aspect ratio, but the value of the maximum lift coefficient and the corresponding angle of attack increases. For the wing with $\varphi = 76$ deg, lift and drag curves, maximum lift coefficients, and corresponding angles of attack are similar for both Mach numbers. Also, in both cases the maximum lift is reached at the angle of attack where the vortex bursts at the wing trailing edge. Since the center of pressure of the wing moves downstream with increasing Mach number, the pitching moment is more negative (nose down) for larger values of the freestream Mach number. The $\varphi = 70$ deg wing shows not only changes on pitching moment, but also the lift slope is larger for the higher Mach number. The maximum lift coefficients are similar for both Mach numbers, but it is obtained at a lower value of the angle of attack for the higher freestream Mach. However, the onset of the vortex breakdown at the wing trailing edge is not influenced by the change in freestream Mach number.

Finally, the wing with $\varphi = 60$ deg exhibits the largest Mach number effects. For low and medium angles of attack the lift slope increases as the Mach number increases. The onset of the vortex breakdown at the trailing edge take place at approximately the same angle of attack for both freestream Mach numbers ($\alpha \cong 15$ deg), but the aerodynamic behavior at larger angles is totally different. On the one hand, for the low Mach number case the lift continues to increase at the same rate and later decays smoothly. Maximum lift for $M_\infty = 0.4$ is reached once the leading-edge vortex is totally bursted above the wing. On the other hand, for the high Mach number the lift slope shows first a sudden drop followed by a flat recovery. This behavior for the $M_\infty = 0.8$ case is due to the fast upstream shift of the vortex bursting location with increasing angle of attack, as is shown in Fig. 4. This faster upstream progression of the breakdown for the wing $\varphi = 60$ deg produces a large loss of vortex lift. Since this phenomenon starts at a relative small incidence, the loss of vortex

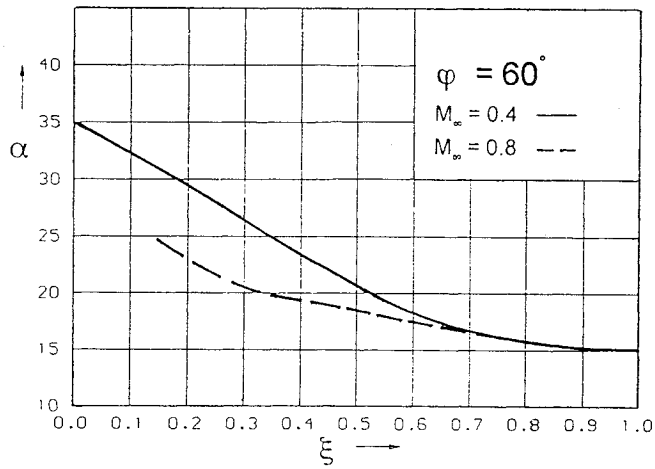

Fig. 4 Effect of the Mach number on the vortex bursting progression for the wing $\varphi = 60$ deg.

lift can not be compensated for by the pressure increase along the lower surface of the wing. As the angle of attack increases, the loss of lift on the lee side of the wing becomes partially compensated by a gain of lift from the windward side, producing a flat recovery of the lift curve. The drag and pitching moment curves show a similar behavior.

Shock-Vortex Interaction

Figure 5 shows iso-C_p lines for the $\varphi = 60$ deg wing at $M_\infty = 0.8$ and angles of attack where the slope of the lift curve experiences the major changes. Also, the figure shows some streamlines with the corresponding values of the local Mach numbers to recognize possible occurrence of shock waves. Supersonic and subsonic flow areas are distinguished by means of white and grey colors, respectively. At $\alpha = 14$ deg (short before the beginning of the vortex breakdown at the wing trailing edge), the flow underneath the leading-edge vortex is fully supersonic, and also there is a small sonic area close to the

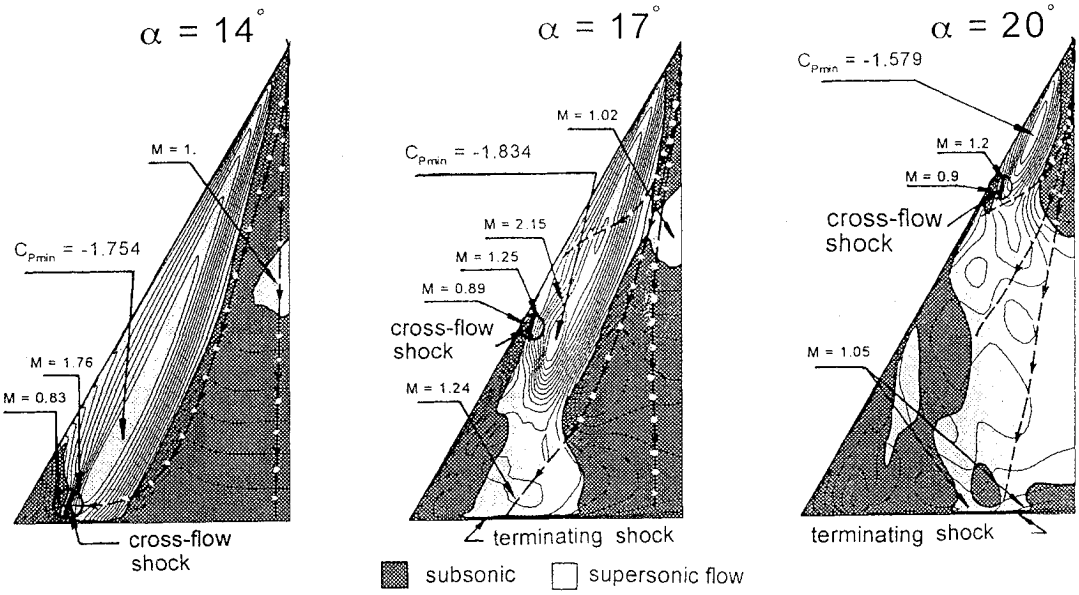

Fig. 5 Effect of the angle of attack on the transonic vortex flow, iso-C_p for the wing φ = 60 deg, M_∞ = 0.8.

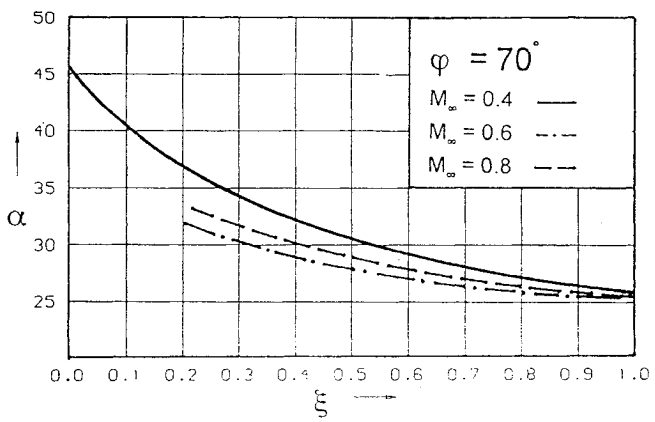

Fig. 6 Effect of the Mach number on the vortex bursting progression for the wing φ = 70 deg.

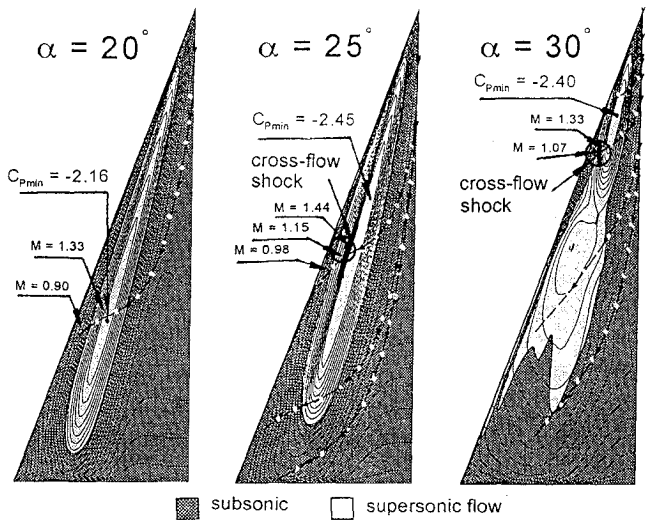

Fig. 7 Effect of the angle of attack on the subsonic vortex flow iso-C_p for the wing φ = 70 deg, M_∞ = 0.6.

symmetry plane. There are no terminating or rear shocks above the wing, but a small strong crossflow shock is developed close to the wing trailing edge. At higher angles of attack this crossflow shock moves upstream together with the point of the vortex bursting. Downstream of the vortex bursting the flow remains supersonic but it is oriented towards the wing trailing edge and, hence, there a terminating shock compresses the flow to the freestream pressure. The upstream shifting of the vortex breakdown together with the crossflow shock continues as the angle of attack increases. Whereas the terminating shock appears after the breakdown of the vortex, the role of the crossflow shock on the onset of the vortex breakdown and its upstream shifting is not clear. To clarify this aspect, Figs. 6–8 display a similar analysis for the wing with $\varphi = 70$ deg. The onset of vortex breakdown at the wing trailing edge for $0.4 \leq M_\infty \leq 0.8$ begins at approximately the same angle of attack ($\alpha \cong 25$ deg), but the upstream shifting of the vortex bursting is faster for freestream Mach numbers larger than 0.4 (see Fig. 6).

In Fig. 7 the pressure fields for $M_\infty = 0.6$ indicate that the flow close to the wing trailing edge is fully subsonic for the angle of attack where the onset of vortex bursting is at wing trailing edge ($\alpha \cong 25$ deg). Moreover, only a weak crossflow shock is present in the field at $\xi \cong 0.5$, underneath the leading-edge vortex. By increasing the angle of attack the vortex breakdown shifts upstream as does the crossflow shock. Close to the wing trailing edge the flow remains subsonic. Supersonic flow at the wing surface is only observed underneath the vortex core and also downstream the location of vortex breakdown.

Finally, Fig. 8 shows the corresponding solutions for $M_\infty = 0.8$. For $\alpha = 10$ deg the flow underneath the leading-edge vortex is already supersonic. At $\alpha = 20$ deg the supersonic region extends toward the symmetry plane. Furthermore, a strong crossflow shock develops underneath the primary vortex. At the initiation of the bursting process the flow above the wing is almost fully supersonic. A strong crossflow shock lies underneath the leading-edge vortex and extends up to the station $\xi \cong 0.3$. Once the location of vortex breakdown passes the trailing edge in direction to the wing apex ($\alpha > 25$ deg), a terminating shock develops at the trailing edge of the wing. Although the crossflow shock for $M_\infty = 0.8$ is stronger than the corresponding shock for the $M_\infty = 0.6$ case, the upstream progression of the vortex bursting is faster for $M_\infty = 0.6$ than for the $M_\infty = 0.8$ case. In considering Fig. 6 once more, it comes out that there is a nonmonotone Mach number effect on the vortex bursting progression. Future work is required to explain this behavior.

Figure 9 shows flow characteristics for the wing $\varphi = 70$ deg at $\alpha = 20$ deg, for the crosswise plane $\xi = 0.6$ and for different Mach numbers. Also, it indicates that the flow inside the vortex core reaches Mach number values almost two times larger than the freestream Mach number. The core flow is already supersonic for $M_\infty > 0.5$. As the freestream Mach number increases, the region of high-speed core flow grows from the vortex core in the radial

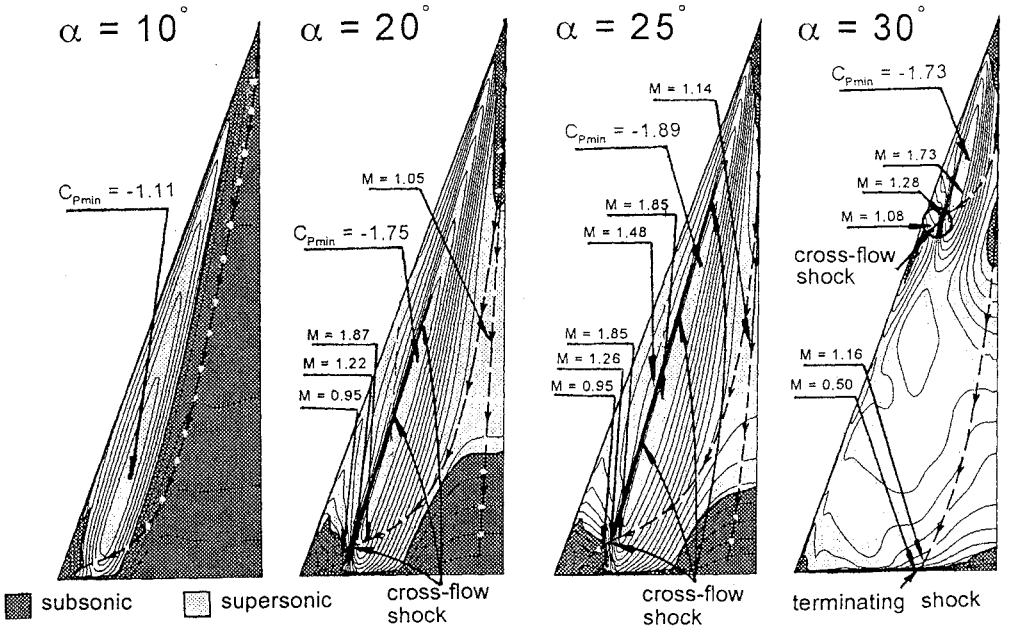

Fig. 8 Effect of the angle of attack on the transonic vortex flow. Iso-C_p for the wing φ = 70 deg, M_∞ = 0.8.

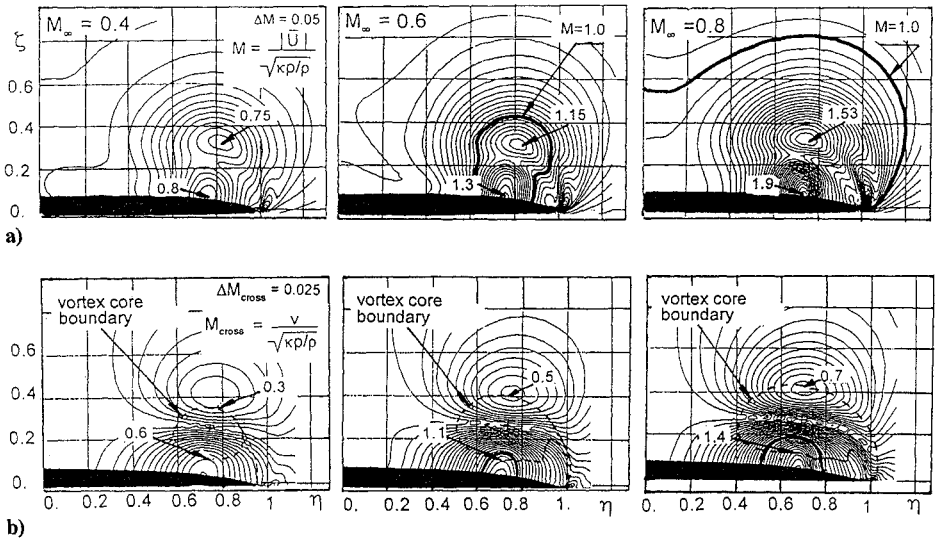

Fig. 9 Iso-Mach lines, wing φ = 70 deg, α = 20 deg: a) local Mach and b) local Mach in spanwise direction.

direction inducing supersonic flow also near the symmetry plane. It turns out that the flow on the upper surface of the wing is mainly oriented in the crosswise direction toward the leading edge of the wing. Only close to the symmetry plane remains a small area with streamwise directed flow where terminating shocks may develop (see also Fig. 8), this possibility being larger for wings with small leading edge swept angles. However, in the present investigation occurrence of terminating shocks was observed only downstream of vortex breakdown. For the wing φ = 60 deg the vortex bursts relatively early for the formation of a terminating shock and for the wings φ = 70 and 76 deg the vortex flow comprises practically the whole upper surface.

Core Flow Effects on Near-Field Wing

Close to the vortex axis Fig. 9a shows that there are two relative maximums of local Mach number of about the same magnitude, one above the vortex axis and one below it close to the wing surface. Considering a local Mach number defined only with the spanwise component of the velocity (Fig. 9b), here denoted as M_{cross} the iso-Mach lines still exhibit two relative maximums but now of different magnitude. Above the vortex axis, M_{cross} is of the same order as M_∞ and, hence, it is a factor too smaller than the corresponding local Mach number at this location. Below the vortex axis, M_{cross} is of the same order as the local Mach number. The flow between the vortex axis and the wing surface may be considered similar to a convergent–divergent channel flow where the subsonic core flow accelerates to supersonic speed. Hence, a crossflow shock already forms underneath the vortex axis for relative low-freestream Mach numbers.

Figure 10 shows the C_p and M_{cross} distributions along generic wall streamlines which cross over the wing station ξ = 0.6 at the position of the maximum suction peak of pressure for different free-stream Mach numbers. Close to the wing apex the flow is oriented in the streamwise direction only. As the streamline is going into the channel, the spanwise component of the Mach number M_{cross} increases. For larger values of the freestream Mach number M_{cross} is supersonic inside the channel. Hence, a crossflow shock develops to compress the supersonic flow to subsonic at the exit of the channel. The location of this crossflow shock is slightly outboard of the vortex axis. Also, as the freestream Mach number increases, the pressure field at the wing upper surface shows an overall increment of the suction values except inside the channel, where for supersonic channel flows the suction values reduce. Thus, for delta wings the behavior of the lift slope with freestream Mach number

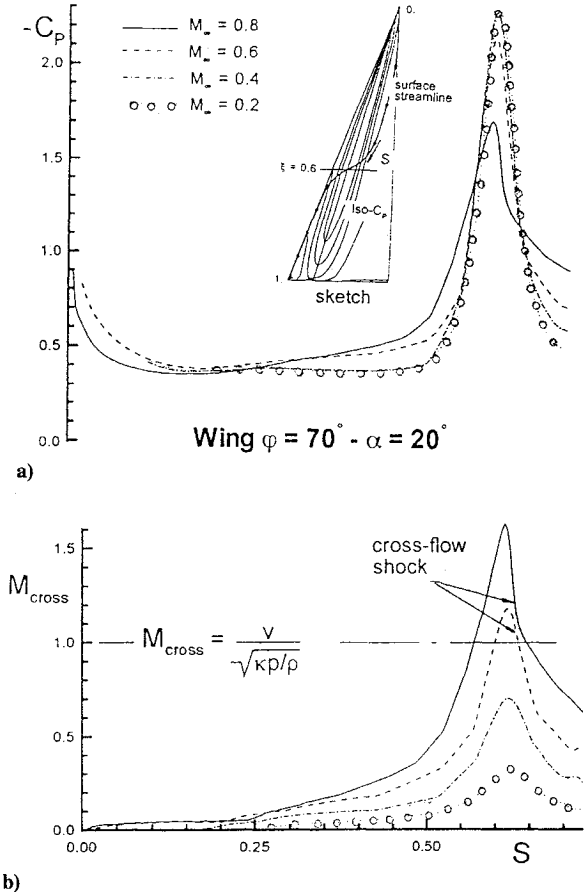

Fig. 10 Flow characteristics along surface stream lines: a) iso-C_p and b) local Mach.

is not necessarily monotonic. Once the freestream Mach number is large enough to induce supersonic flow inside the channel, the lift coefficient may still increase, remain, or start to decrease depending on the amount of the vortex lift relative to the overall lift of the delta wing. For delta wings with small swept leading-edge angles, like the wing $\varphi = 60$ deg, i.e., wings with small ratio vortex lift-overall lift, an increase in the freestream Mach number produces an increase of the lift coefficient. On the other hand, for wings with large vortex lift-overall lift ratios (wing $\varphi = 76$ deg) an increment on the freestream Mach number from $M_\infty = 0.4$ to 0.8 produces no marked changes on the lift curves.

Finally, Fig. 11 shows the types of flow experimentally found on sharp leading-edged delta wings[24] and the boundaries between them, displayed in a plane of M_N and α_N, where M_N is the Mach number component normal to the wing leading-edge defined as $M_N = M_\infty(1 - \sin^2\varphi\cos^2\alpha)^{0.5}$. Also, recent experimental data[3,4] are included where early occurrences of crossflow shocks are reported. The present investigation shows that for inviscid flows crossflow shocks already develop for $M_N \cong 0.4$ for a large spectrum of angles of attack. The occurrence of embedded shocks beneath vortices found in the present study is shaded in gray in Fig. 11. It would be interesting to account for this numerical finding in future experimental studies.

Wing Effects on Near-Field Core Flow

In this section the study is carried out on a vortex oriented coordinate system. Accordingly, the origin of coordinates is located at the wing apex, the x axis is aligned with the vortex axis, and the y axis, perpendicular to the x axis, is parallel to the plane of the wing planform. Finally, the z axis is normal to the plane defined by the other two axes. In this coordinate system the velocity components u, v, and w are denoted as axial, transversal and normal velocity components. Although the results here discussed are only for the wing $\varphi = 70$ deg for $\alpha = 20$ deg case, the conclusions apply for the family of delta wings of the present study.

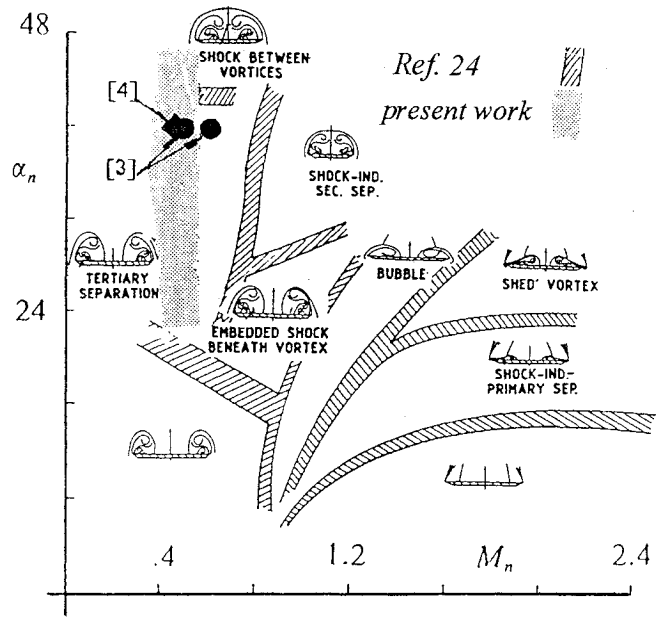

Fig. 11 Flow boundaries for sharp-edged delta wings from Ref. 24.

Figure 12 shows flow pictures of lines of constant velocities for two Mach numbers, $M_\infty = 0.1$ and 0.8. They are plotted in a plane perpendicular to the vortex axis, which cross the point $\xi = 0.6$ at the symmetry plane of the wing. At the vortex axis the axial velocity exhibits a maximum, whereas the other two components vanish. The flow motion is not rotationally symmetric in this reference system aligned with the vortex axis. In the case of vortex flow motions with no radial velocity component, the flow picture for the isovelocity lines $(v^2 + w^2)^{\frac{1}{2}}$ should be concentric circles with the vortex axis at the center. Figure 12 reveals that the inviscid vortex flow motion of a delta wing is not free of radial velocities. On the contrary, within the vortex core there are strong radial forces necessaries to establish the spiraling flow.[25]

Comparing the magnitude of the normal component with the magnitude of the transversal component of the velocity shows that the maximum values of the v component of the flow motion are almost two times larger than the maximum values of the w component due to the channel formed between the vortex core and the wing surface. The isolines of total velocity indicate that within the vortex core and in its vicinity, the flow is already compressible even for $M_\infty = 0.1$. Because of the lack of rotational symmetry, the total velocity of the flow motion exhibits an absolute maximum below the vortex axis. A relative maximum of the total velocity is observed above the vortex axis whereas there is a relative minimum at the vortex axis. The difference in the maximums of total velocity found above and below the vortex axis, relative to the velocity exhibited at the vortex axis, tends to reduce as the freestream Mach number increases. The discretization error of the numerical simulation may also enlarge these deficits in velocity, as was already shown in Ref. 10. The present simulations exhibit approximately a 15% deficit in total velocity at the vortex axis, which is more or less freestream Mach number independent. The presence of the wing surface on the near field of the vortex core leads to an acceleration of the vortical flow motion in the crosswise direction, which introduces strong radial forces. The vortex core deforms under the action of the resulting different centrifugal forces acting at top and bottom. The resulting vortex core shape is rather flat. Also, considering that vorticity is simply twice the angular velocity and that radial forces are the source of the angular velocities, in addition to the vorticity fed from the leading edge, vorticity is also generated within the vortex core.

Figure 13 shows that the main source of vorticity in the field is the leading-edge of the wing. There, the magnitude of the vorticity is about 27 times larger than at the vortex axis. At the vortex core the axial component of the vorticity is almost the total amount of vorticity found within the core. The other two components are almost five times smaller, and they act only at the outer boundary of

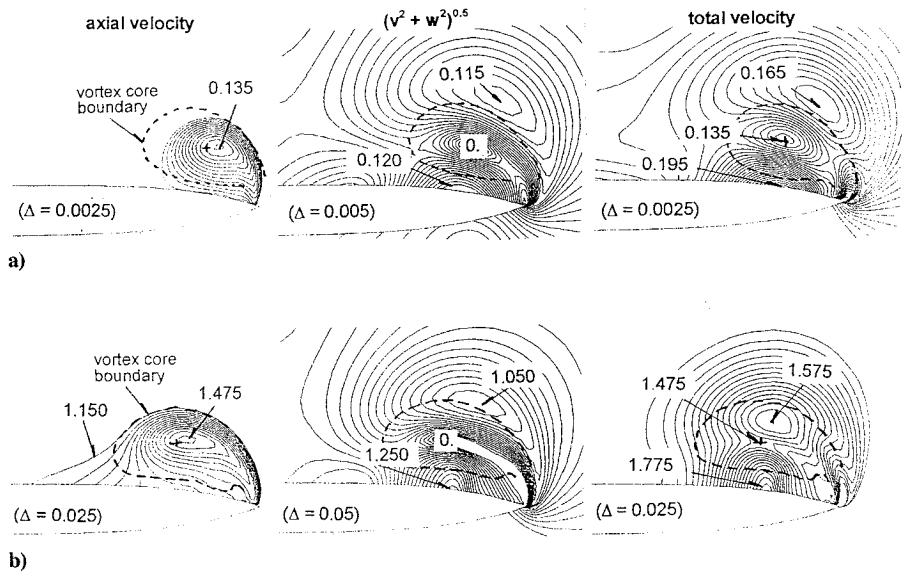

Fig. 12 Isovelocity lines, wing φ = 70 deg, α = 20 deg: a) M_∞ = 0.1 and b) M_∞ = 0.8

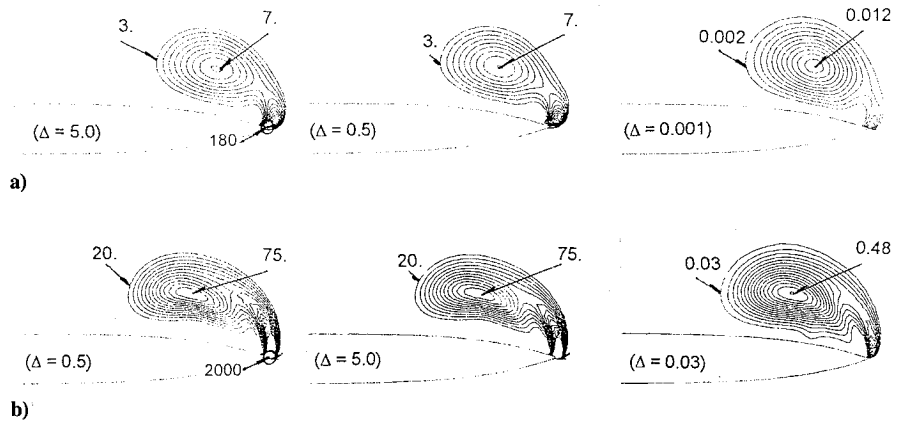

Fig. 13 Isovorticity and total pressure loss lines, wing φ = 70 deg, α = 20 deg: a) M_∞ = 0.1 and b) M_∞ = 0.8.

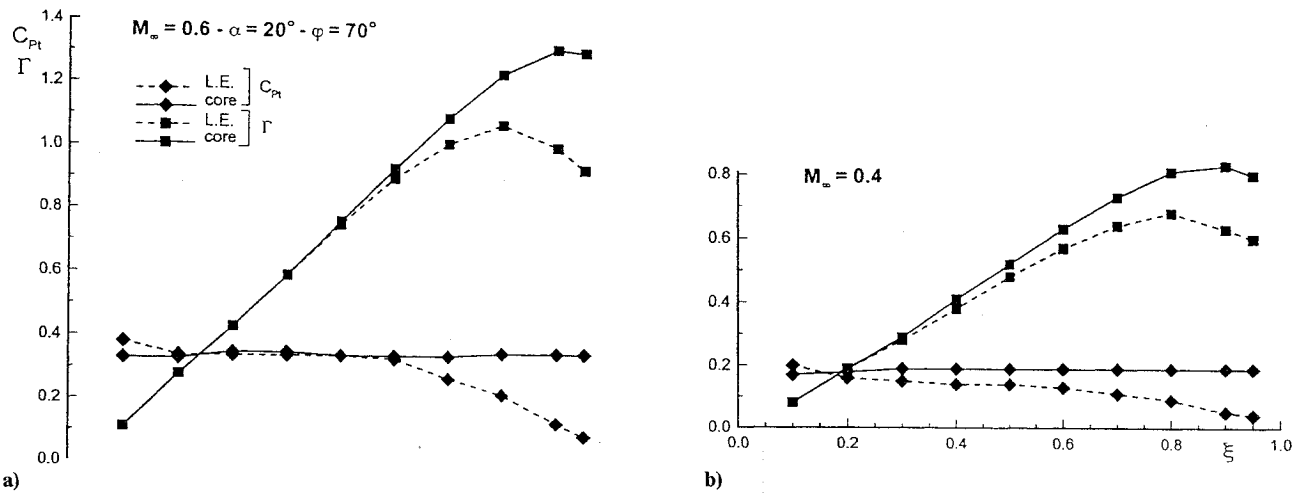

Fig. 14 Circulation and total pressure losses computed at the wing leading edge and at the vortex core for the wing φ = 70 deg, α = 20 deg, for two freestream Mach numbers.

the vortex core. The definition of the axial vorticity component is $\gamma_x = \partial v/\partial z - \partial w/\partial y$. Because of the channel flow formed between the wing and the vortex core, $\partial v/\partial z$ is about five times larger than $\partial w/\partial y$. Also, Fig. 13 shows that within the vortex core the total pressure is not conserved. For calorically perfect gas these losses of total pressure experienced by the gas are equal to entropy changes. According to Crocco's theorem, in three-dimensional rotational flows positive entropy gradients ∇S are related to the cross product of the vorticity vector Ω with the velocity vector $\bar{V}$ i.e., $\nabla S \approx \bar{\Omega} \times \bar{V}$.

Figure 14 shows maximum local values of the circulation and total pressure loss computed at the wing leading edge and at the vortex axis from the apex to the trailing edge, for the wing φ = 70 deg

for two Mach numbers, $M_\infty = 0.4$ and 0.6. It is shown that the production of circulation at the wing leading edge varies linearly with distance from the wing apex up to close to the wing trailing edge, where its decays. At the vortex axis the circulation increases in a similar way to that at the wing leading-edge, but as the vortex moves away from the wing surface, in traveling from the apex to the wing trailing edge, the amount of circulation computed at the vortex core is larger than that computed at the wing leading edge. Whereas for $M_\infty = 0.4$ this phenomena already starts beyond $\xi = 0.3$, for $M_\infty = 0.6$ the vortex core lies closer to the wing surface and, hence, a delay of this phenomena to farther downstream stations is observed. Thus, besides the convection of circulation from the wing leading-edge, circulation is generated within the vortex core as the distance between vortex core and wing surface increases. Also, the entropy gradients computed at the vortex core are partially due to convection of entropy from the wing leading edge and partially due to the misalignment of the velocity and vorticity vectors there. Figure 13 showed that within the inviscid vortex core the vorticity vector is tangential to the vortex axis whereas according to Fig. 12 the velocity vector has a resulting direction toward the wing surface. In moving from the apex to the wing trailing edge the local values of losses of total pressure computed at the wing leading edge (see Fig. 14) decrease whereas the local values computed at the vortex core remain constant. The reduction on the entropy gradients convected from the leading edge is being compensated for at the vortex core, resulting in values of entropy gradients nearly constant along the vortex axis.

Conclusions

The inviscid compressible leading-edge vortex flow of a sharp-edge delta wing was studied by means of the numerical solution of the Euler equations. Solutions were obtained for three delta wings with sweep leading-edge angles of $\varphi = 60$, 70, and 76 deg for freestream Mach numbers $0.1 \leq M_\infty \leq 0.8$, and for angles of attack up to vortex breakdown.

The present investigation has shown that the onset of vortex breakdown at the trailing edge of the wing is only weakly influenced by the freestream Mach number for the present Mach number range ($M_\infty \leq 0.8$), but the upstream progression of the vortex bursting with incidence is faster for supersonic than for subsonic core flows, even for flows free of shock waves. Terminating or rear shocks are observed downstream of vortex bursting in transonic flows. Furthermore, a convergent–divergent channel type flow is formed between the wing surface and the vortex axis which accelerates the subsonic flow to supersonic speeds. Crossflow shocks may be formed within the channel for freestream Mach numbers with a normal component to the wing leading edge as low as $M_N \cong 0.4$ for a large spectrum of angles of attack. As the velocity in the channel becomes supersonic, the induced suction peak of pressure on the wing surface underneath the leading edge vortex is reduced.

Also, it is shown that the core flow is compressible for freestream Mach numbers $M_\infty \approx 0.1$. The presence of the wing introduces strong radial velocities which lead to a nonuniform distribution of total velocity within the core. Because of the different magnitudes of the centrifugal forces acting on the top and the bottom of the core, it deforms and has a rather flat shape. Furthermore, besides convection of circulation and entropy from the wing leading-edge, significant amounts of circulation are generated within the vortex core which depend on the relative distance of the core to the wing surface.

Acknowledgments

This investigation was partially funded as a joint-program of the DLR-BS and the aerospace company DASA-München. The author also thanks A. Das and D. Hummel for the many helpful discussions.

References

[1]Hoeijmakers, H. W. M., "Modeling and Numerical Simulation of Vortex Flow in Aerodynamics," AGARD CP-494 Paper 1, July 1991.

[2]Newsome, R. W., and Kandil, O. A., "Vortical Flow Aerodynamics—Physical and Numerical Simulation," AIAA Paper 87-0206, Jan. 1987.

[3]Elsenaar, A., Bütefisch, K., Hjelmber, L. and Bannink, W. J., "The International Vortex Flow Experiment," AGARD CP-437 Paper 9, April 1988.

[4]Erickson, G. E., Schreiner, J. A., and Rogers, L. W., "Canard-Wing Vortex Interactions at Subsonic Through Supersonic Speeds," AIAA Paper 90-2814, Aug. 1990.

[5]McMillan, S. N., Thomas, J. L., and Murman, E., "Navier–Stokes and Euler Solutions for Lee-Side Flows Over Supersonic Delta Wings—A Correlation With Experiments," NASA TP-3035, Dec. 1990.

[6]Longo, J. M. A., "Simulation of Complex Inviscid and Viscous Vortex Flows," *IUTAM Symposium on Fluid Dynamic of High Angle of Attack*, edited by R. Kawamura, and Y. Aihara, Springer-Verlag, Berlin, 1993, pp. 363–373.

[7]Murman, E., and Rizzi, A., "Application of Euler Equations to Sharp Edge Delta Wings with Leading Edge Vortices," AGARD CP-412 Paper 15, Nov. 1986.

[8]Hitzel, S., "Wing Vortex-Flows Up into Vortex-Breakdown—A Numerical Simulation," AIAA Paper 88-2518, June 1988.

[9]O'Neil, P. J., Barnett, R. M., and Louise, C. M., "Numerical Simulation of Leading-edge Vortex Breakdown Using an Euler Code," AIAA Paper 89-2189, July 1989.

[10]Longo, J. M. A., "The Role of the Numerical Dissipation on the Computational Euler Equations Solutions for Vortical Flows," AIAA Paper 89-2232, July 1989.

[11]Raj, P., Sikora, J. S., and Keen, J. M., "Free-Vortex Flow Simulation Using a Three-dimensional Euler Aerodynamic Method," ICAS Paper 86-1.5.2, 15th International Council of the Aeronautical Sciences, England, UK, Sept. 1986.

[12]Longo, J. M. A., and Das, A., "Numerical Simulation of Vortical Flows over Close-Coupled Canard-Wing Configuration," AIAA Paper 90-3003, Aug. 1990.

[13]Hoeijmakers, H. W., Jacobs, J. M. J. W., and Van den Berg, J. I., "Numerical Simulation of Vortical Flows over a Delta Wing at Subsonic and Transonic Speeds," ICAS Paper 90-3.3.3, 17th International Council of the Aeronautical Sciences, Sweden, Sept. 1990.

[14]Agrawall, S., Barnett, R. M., and Robinson, B. A., "Investigation of Vortex Breakdown On a Delta Wing Using Euler and Navier–Stokes Equations," AGARD CP-494 Paper 24, July 1991.

[15]Malfa, E., Guarino, L., and Visintini, L., "Application of Euler Equations to the Computation of Vortex Flows on Wing-Body and Close-Coupled Wing-Body-Canard Configurations," AIAA Paper 91-3306, Sept. 1991.

[16]Longo, J. M. A., "Numerische Analyse der Strömungsfelder von Deltaflügelkonfigurationen ohne und mit Canard," Zentrum für Luft und Raumfahrttechnik, Technische Universität Braunschweig, Germany ZLR-Forschungsbericht 93-09, Oct. 1993.

[17]Radespiel, R., "A Cell-Vertex Multigrid Method for the Navier–Stokes Equations," NASA TM-101557, Jan. 1989.

[18]Atkins, H., "A Multiple-Block Multigrid Method for the Solution of the Euler and Navier–Stokes Equations," AIAA 91-0101, Jan. 1991.

[19]Rossow, C. C., "Efficient Computation of Inviscid Flow Fields Around Complex Configurations Using a Multi-Block Multigrid Method," *Communications in Applied Numerical Methods*, Vol. 8, edited by John Wiley & Sons, Ltd., 1992, pp. 735–747.

[20]Jameson, A., Schmidt, W., and Turkel, E., "Numerical Solutions of the Euler Equations by Finite Volume Methods Using Runge–Kutta Time Stepping Schemes," AIAA Paper 81-1259, June 1981.

[21]Wendz, W. H., Jr., and Kohlman, D. L., "Vortex Breakdown on Slender Sharp-Edged Wings," *Journal of Aircraft*, Vol. 8, No. 3, 1971, pp. 156–161.

[22]Oelker, H.-C., and Hummel, D., "Investigation on the Vorticity Sheets of a Close Coupled Delta-Canard Configuration," ICAS Paper 88-3.11.RI, 16th International Council of the Aerospace Sciences, Israel, Sept. 1988.

[23]Erickson, G. E., "Flow Studies of Slender Wing Vortices," AIAA Paper 80-1423, July 1980.

[24]Narayan, K. Y., and Seshadri, S. N., "Vortical Flows on the Lee Surface of Delta Wings," *IUTAM Symposium Transsonicum III*, edited by J. Zierep, and H. Oertel, Springer-Verlag, Berlin 1988, pp. 329–338.

[25]Das, A., "Analysis of Spiraling Vortical Flows around Slender Delta Wings Moving in an Inviscid Medium," *ZAMM Zeitschrift für Angwandte Mathematik und Mechanik*, Vol. 71, No. 11, 1991, pp. 465–471.